**Supplementary Information**

**Supplemental Data**

**Supplemental figure 1: Disrupted MN cannot retain nuclear proteins, are present in RPE-1 cells, and occur throughout interphase and independently of MN size or origin, related to Figure 1.** (A) Images of asynchronous U2OS GFP-NLS cells expressing NES-tdTomato (tdTom)-NLS labeled with antibodies to lamin A (LmnA) after treatment with DMSO or leptomycin B for 1 h. For all images arrows indicate intact MN, arrowheads indicate disrupted MN. All scale bars = 10 μm. (B) Quantification of MN integrity and localization of NES-tdTom-NLS to MN after 1 h incubation in leptomycin B. N = 300 MN from 3 experiments. P = p-value as determined by Fisher's exact test and $\phi$ = correlation coefficient. (C) Image of RPE-1 GFP-NLS cells 24 h post mitotic shake-off labeled with anti-LmnA. (D) Quantification of time MN remain intact after NE formation (M1) in U2OS GFP-NLS cells analyzed by time-lapse imaging as a proportion of the total time the cell is in interphase, ending at NE breakdown (M2). The median (shown) = 0.37. N = 44 MN. (E) Quantification of MN integrity in U2OS GFP-NLS cells synchronized by mitotic shake-off into medium containing either hydroxyurea (HU) or RO-3306 and fixed at the times indicated. N = 300 MN/time point. (F) Quantification of MN integrity in RPE-1 GFP-NLS cells incubated in nocodazole and synchronized by mitotic shake-off into medium containing EdU. Only MN in cells with EdU negative PN were counted. N = 300 MN/time point from 3 experiments. (G) Comparison of initial MN area versus MN fate. U2OS GFP-NLS cells were observed by time-lapse imaging and MN area recorded when decondensation was complete. Mean and 95 % confidence interval (CI) are shown on graph. Means are not significantly different ($p > 0.05$) by 1-way ANOVA. N = 118 MN from 2 experiments. (H) Representative images of disrupted MN in fixed U2OS GFP-NLS cells labeled with human anti-centromere-auto-antigen (ACA). Images are maximum intensity projections of 6.39 μm (top) and 5.41 μm (bottom) z-stacks. (E) Quantification of MN integrity in MN with or

without centromere (Cent.) labeling. N = 300 MN/category from 3 experiments. Populations are not significantly different ($p > 0.05$) by Fisher's exact test.

**Supplemental figure 2: Disrupted MN retain some nucleoporins, have compacted chromatin, and accumulate a trans-membrane ER protein, related to Figure 2.** (A) Representative images of the anti-nuclear pore antibody mAB414 (414) labeling in intact (arrow) and disrupted (arrowhead) MN in U2OS GFP-NLS cells. All scale bars = 10 μm. (B) Quantification of fluorescence intensity of mAB414 labeling at the nuclear rim in intact and disrupted MN expressed as a ratio of mean fluorescence intensity between MN and PN in the same cell. N = 31 MN/category from 3 experiments. Mean and 95 % CI are shown on graph. Means are not significantly different ($p > 0.05$) by t-test. (C and D) Cells analyzed as for (A and B) using antibodies to the nuclear pore basket proteins Nup153 and TPR. * indicates a significant ($p < 0.05$) difference between intact and disrupted MN fluorescence intensity ratios by t-test. Mean and 95 % CI are shown on graph. (E) Stills from time-lapse imaging of U2OS RFP-NLS cells expressing Sec61B-GFP and labeled with Hoechst prior to imaging to mark DNA. Prior to disruption the MN is marked by an arrow and post disruption by arrowheads. Disruption occurs at t = 0. Time is h:m. (F) Images of U2OS RFP-NLS cells expressing Sec61B-V5 and labeled with antibodies to calreticulin (CalR). (G) Quantification of DAPI fluorescence intensity in intact and disrupted MN in fixed cells as described for (B). N = 25 MN per category. Mean DAPI intensity (shown on graph with 95% CI) is significantly different (* = $p < 0.05$) between intact and disrupted MN by t-test. (H) Comparison of the areas of intact and disrupted MN determined by DAPI staining. Mean area (shown on graph with 95% CI) is significantly different (* = $p < 0.05$) between intact and disrupted MN by t-test. N > 64 MN per category. (I) Images of intact (arrow) and disrupted (arrowhead) MN in U2OS GFP-NLS cells labeled with antibodies to acetyl-histone3-K9 (H3K9Ac). The p and ϕ values are from quantification of the

proportion of intact and disrupted MN labeled with antibodies to H3K9Ac. P-value determined by Fisher's exact test. N = 300 MN/category from 3 experiments.

**Supplemental figure 3: MN disruption is not affected by loss of lamins A or B2 and controls related to Figure 3.** (A) Western blot of all three lamins in the indicated stable cell lines (bottom). Antibodies used for immunoblotting are listed at right. Numbers at top represent quantification of affected lamin levels normalized to the control "none" shRNA cell line. Fractions represent LmnB1, LmnA, and LmnB2 levels, in order. N = 3. (B and C) Quantification of MN integrity (Dis. = disrupted) in asynchronous U2OS GFP-NLS cells expressing indicated shRNA. N = 300 MN/cell line from 3 experiments. P-values from Fisher's exact tests were non-significant ($p>0.05$). (D) Western blot of U2OS GFP-NLS cells expressing indicated shRNAs and transfected with indicated siRNAs. Numbers at top represent relative LmnB1 levels. N = 3. (E) Quantification of MN integrity in cell lines shown in (D). P-values at top are the result of Fisher's exact tests on indicated samples. N = 300 MN/cell line from 3 experiments. (F) Images of U2OS GFP-NLS cells expressing mCherry or mCherry-LmnB1-ND (non-degradable) and labeled with anti-LmnB1 antibodies. All scale bars = 10 μm. (G) Western blot of U2OS GFP-NLS cells expressing (Exp.) indicated proteins and shRNA. mCh= mCherry and ND = non-degradable. Top numbers indicate fraction of total LmnB1 expression compared to "None". N =3. (H) Images of intact (arrows) and disrupted (arrowheads) MN in mCherry or mCherry-LmnB2 U2OS GFP-NLS cell lines labeled with anti-LmnB1. (I) Western blot of U2OS GFP-NLS mCherry and U2OS GFP-NLS mCherry-LmnB2 cell lines. Numbers at top indicate relative LmnB2 expression. N = 3.

**Supplemental figure 4: Disrupted MN fail to transcribe mRNA, are not associated with apoptosis, and show cell-cycle dependent γ-H2AX accumulation, related to Figure 4.** (A) Images of intact (arrow) and disrupted (arrowhead) MN after RNA fluorescent *in situ*

hybridization using an oligo-dT probe. Images are maximum intensity projections of 6.74 μm (top) and 3.37 μm (bottom) z-stacks. All scale bars = 10 μm. (B) Quantification of proportion of γ-H2AX labeled MN in asynchronous U2OS GFP-NLS mCherry (mCh) or mCherry (mCh)-LmnB2 cells. N = 300 MN/cell line from 3 experiments. p = p-value from Fisher's exact test. (C) Quantification γ-H2AX labeling in disrupted MN in U2OS GFP-NLS cells synchronized by mitotic shake-off. Cell cycle states determined as in Figure 1G. N = 300 MN/time point. P-values at top were determined by Fisher's exact and $\chi^2$ analyses of indicated samples. (D) Images of cleaved caspase-3 and γ-H2AX labeling in an apoptotic cell and a cell containing disrupted MN (arrowhead).

**Supplemental figure 5: Disrupted MN in NSCLC lose TPR and acetyl-histone3K9 and are not associated with apoptotic cells, related to Figure 6.** (A) Image of NSCLC section labeled with TPR, E-cadherin, and γ-H2AX. A γH2AX positive disrupted MN (arrowhead) lacks TPR labeling although intact MN (arrows) and the PN in the same cell have TPR at the nuclear rim. All scale bars = 10 μm. (B) γ-H2AX positive MN lack acetyl-histone3-K9 (H3K9Ac) in NSCLC. Representative image of a disrupted MN (arrowhead), identified by γ-H2AX and E-cadherin labeling, also labeled with anti-H3K9Ac. Image is a maximum intensity projection of a 7.37 μm z-stack. (C) Disrupted MN are distinguishable from apoptotic cells. Images of an apoptotic cell, identified by cleaved capsase-3 labeling, and a cell containing a disrupted MN in NSCLC sections labeled with antibodies against cleaved caspase-3, E-cadherin, and γ-H2AX. Images are maximum intensity projections of 7.37 μm (top) and 9.34 μm (bottom) z-stacks.

**Movie S1. Time-lapse imaging of MN disruption, related to Figure 1.** U2OS 2xRFP-NLS cells expressing 4xGFP-NES and labeled with Hoechst were imaged for 30 h and images were

acquired every 3 min using a 20x objective. Movie panels represent Hoechst, GFP, RFP, and merged channels, in order. Scale bar = 10 μm. One second = 45 minutes real time.

**Movie S2. Kinetics of NE rupturing and repair in the PN, related to Figure 2.** U2OS GFP-IBB, H2B-mCherry cells were observed for 6 h by time-lapse imaging. The PN ruptures twice at its top during the movie. Images were acquired every 33 s using a 20x objective. One second = 8.1 minutes real time.

**Movie S3. Kinetics of MN disruption, related to Figure 2.** Images of a U2OS GFP-IBB, H2B-mCherry cell acquired with the same conditions as Movie S2.

**Movie S4. NE and chromatin collapse after MN disruption, related to Figure S2.** U2OS RFP-NLS (red, top right) cells expressing Sec61B-GFP (green, bottom left) and labeled with Hoechst (blue, top left) were imaged for 24 h. Images were acquired every minute using a 20x objective. One second = 15 minutes real time.

**Movie S5. Lamina morphology changes in interphase MN, related to Figure 3.** U2OS RFP-LmnB1 GFP-NLS cells were imaged for 30 h. Images were acquired as a 2.5 μm z-stack with 0.5 μm steps every 3 minutes using a 63x objective. Movie represents a maximum intensity projection at each time point. Movie panels are GFP, RFP, and merged channels, in order. One second = 45 minutes real-time. MN begins with a continuous lamina, which forms an enlarging hole prior to MN disruption.

**Movie S6. Lamina morphology in MN after mitosis, related to Figure 3.** Images of a U2OS RFP-LmnB1 GFP-NLS cell acquired and presented with the same conditions as Movie S5. A hole in the lamina is visible shortly after mitosis and persists until MN disruption.

## Extended experimental procedures

### Plasmids

2xRFP-NLS (RFP-NLS) was made by recombination of a PCR of TagRFP (Evrogen) fused to a C-terminal NLS (PPKKKRKV) into the Gateway vector pDONOR20 and recombining into pcDNA-DEST53-mCherry to generate mCherry-TagRFP-NLS. 3xGFP-NLS (GFP-NLS) was previously described (Vargas et al., 2012), and contains EGFP-NLS (PPKKKRKV)-EGFP in the Gateway vector pcDNA-DEST53. 4xGFP-NES (GFP-NES) was made by a PCR of 3 EGFPs separated by 15 nt linker sequences to an N-terminal NES (LQLPPLERLTL) into pDONOR207 and recombining into pcDNA-DEST53 to generate $GFP_{C3}$-NES-3xEGFP. NES-tdTomato-NLS was previously described (Doucet et al., 2010). H2B-mCherry and 3xGFP-IBB (GFP-IBB) were gifts of M. Schmitz and D. Gerlich (Steigemann et al., 2009; Schmitz et al., 2010). pIRES3puro:3xGFP-NLS was made by subcloning 3xGFP-NLS from the Gateway vector backbone into pIRES3puro. pQCXIB-3xGFP-NLS was made by PCRing 3xGFP-NLS from the plasmid 3xGFP-NLS and ligating into pQCXIB_CMV_TO_DEST with the Gateway cassette removed. Sec61B-GFP contains full-length human Sec61B in the Gateway vector pcDNA-DEST47. V5-Rtn3 was previously described (Anderson and Hetzer, 2008a) and contains full-length human Rtn3 cDNA in the Gateway vector pcDNA6.2/N-V5 Lumio DEST. Sec61B-V5 was made by recombining Sec61B into pcDNA6.2/C-V5 Lumio DEST. ER-GFP (ss-GFP-KDEL) was the gift of E. Snapp. pQCXIB-mCherry-LmnB2 was made by ligating PCRs of mCherry and human lamin B2 long, a gift from H. Herrmann (Schumacher et al., 2006), into pQCXIB_CMV_TO_DEST with the Gateway cassette removed. LmnB1-ND (non degradable) was made introduction of synonymous mutations in the targeted region by site directed mutagenesis. The original sequence CGC ATG AGA ATT GAG AGC CTT was changed to CGG ATG AGG ATA GAA ACT CTA. LmnB1-ND was then recombined into pcDNA-DEST53 mCherry.

The sequence of the lamin B1 siRNA used (Life Technologies) was CGC GCU UGG UAG AGG UGG ATT. The control siRNA (Life Technologies) sequence was UAG ACA CCA UGC ACA AUC CTT.

**Stable Cell Lines**

Stable cell lines used in this study were U2OS GFP-NLS (Vargas et al., 2012), U2OS RFP-NLS, HeLa GFP-NLS, DU145 GFP-NLS, MDA-MB-231 GFP-NLS, hTERT RPE-1 GFP-NLS, U2OS GFP-IBB H2B-mCherry (Anderson et al., 2009), U2OS shRNA-LmnB1 GFP-NLS (Vargas et al., 2012), U2OS shRNA-LmnA/C GFP-NLS, U2OS GFP-NLS RFP-LmnB1, U2OS shRNA LmnB2 GFP-NLS RFP-LmnB1, U2OS GFP-NLS mCherry, and U2OS GFP-NLS mCherry-LmnB2.

U2OS GFP-NLS cells were made by transfecting U2OS cells with 3xGFP-NLS, selecting with 0.5 mg/mL G418 for two weeks, and collecting the GFP+ population by FACS. U2OS RFP-NLS cells were made similarly starting with U2OS cells transfected with 2xRFP-NLS. HeLa GFP-NLS, DU145 GFP-NLS, MDA-MB-231 GFP-NLS and RPE-1 GFP-NLS were made by infecting cells with retrovirus made from pQCXIB-3xGFP-NLS, selecting with 2 μg/mL puromycin, and collecting positive cells by FACS. U2OS GFP-IBB H2B-mCherry cells were made by co-transfecting with H2B-mCherry and 3xGFP-IBB, selecting with G418 and puromycin, and collecting double positives by FACS. U2OS RFP-LmnB1 GFP-NLS cells were made by transfecting U2OS cells containing RFP-LmnB1 tagged at the endogenous locus (Sigma) with pIRES3puro:3xGFP-NLS, selecting with puromycin, and collecting GFP+ cells by FACS .

Lamin B1 was depleted in U2OS GFP-NLS cells by infection with a lentivirus containing PLKO.1:shRNA-LmnB1.71 (NM_005573.2-1258s1c1, Sigma), and selection with puromycin. The sequence of the lamin B1shRNA is: CCGGGCATGAGAATTGAGAGCCTTTCTCGAGAAAGGCTCTCAATTCTCATGCTTTTT. Lamin B2 was depleted in U2OS RFP-LmnB1 GFP-NLS cells by infection with a lentivirus containing

PLKO.1:shRNA-LmnB2 (NM_032737.2-4361s1c1, Sigma), and selection with puromycin. The sequence of the lamin B2 shRNA is: CCGGCGGCAGTTCTTTGTTAAAGATCTCGAGATCTTTAACAAAGAACTGCCGTTTTTG. Lamin A/C was depleted in U2OS GFP-NLS cells by infection with a lentivirus containing PLKO.1:shRNA-LmnA/C (NM_170707.1-885s1c1, Sigma), and selection with puromycin. The sequence of the lamin A/C shRNA is: CCGGCGACTGGTGGAGATTGACAATCTCGAGATTGTCAATCTCCACCAGTCGTTTTTG.

U2OS GFP-NLS mCherry cells were made by co-transfecting U2OS cells with pcDNA-DEST53 mCherry and pIRES3puro:3xGFP-NLS, selecting with G418 and puromycin, and sorting for double positives by FACS. U2OS GFP-NLS mCherry-LmnB2 cells were obtained by infecting U2OS GFP-NLS cells with a retrovirus containing pQCXIB-mCherry-LaminB2, selecting with blasticidin, and single cell colony selection for cells with correct localization.

**Antibodies**

Concentrations are listed as follows: IF = immunofluorescence, coverslips, IF-P = immunofluorescence, paraffin sections, W = western blot. Antibodies used for immunofluorescence and western blotting in this study were: goat anti lamin B1 (IF: 1:500, W: 1,1000; Santa Cruz Biotechnology), rabbit anti lamin A (IF: 1:500, IF-P: 1:200, W: 1:1000 Sigma), mouse anti lamin B2 (IF: 1:2000, W: 1:1000, Abcam), mouse anti GAPDH (W: 1:5000, Abcam), mouse anti phospho-Ser17-LmnB2 (1:1000, gift from T. Tomonaga (Kuga et al., 2010)), rabbit anti TPR (IF: 1:500, IF-P: 1:250; Abcam), mouse anti γ-H2AX (IF: 1:500, IF-P: 1:250; Biolegends), mouse anti E-cadherin (IF-P: 1:250; BD Technologies), mouse anti Nup153, ascites fluid (1:1; gift from B. Burke (Bodoor et al., 1999)), rabbit anti calreticulin (1:100; ThermoFisher Scientific), mouse anti RNAPolIIpS2 (H5) (1:300; Covance), mouse anti retinoblastoma (1:200; Cell Signaling Technology), rabbit anti cyclin A (1:500; gift from T. Hunter (Pines and Hunter, 1990)), rabbit anti cleaved caspase-3 (1:1000; Cell Signaling Technologies), human ACA serum (1:1000; Antibodies Inc.), mAb 414 (1:1000; Covance), rabbit anti acetyl-

histone 3 K9 (IF: 1:400, IF-P: 1:200; Cell Signaling Technologies), mouse anti V5 (1:1000; Life Technologies), rabbit anti LSD-1 (1:200, Cell Signaling Technologies), and rabbit anti biotin (1:1000; Rockland Immunochemicals). Alexa Fluor 680 or 800-conjugated secondary antibodies (Life Technologies) were used at 1:10,000 for western blots. EdU labeling with Alexa-555 was performed using the ClickIT EdU Alexa-555 kit according to manufacturer's instructions (Life Technologies). Primary and secondary antibodies were incubated on coverslips for 30 min each at RT. Primary antibodies were incubated overnight at 4˚C on paraffin sections and secondary antibodies for 30 min at RT. Primary and secondary antibodies were incubated on western blots for 1 h each.

**Image quantifications and statistics**

The dynamics of PN NE rupturing and MN disruption were calculated by measuring mean fluorescence intensity of GFP-IBB for an ROI within the nucleus over the course of a rupturing event. The mean fluorescent intensity was background subtracted and normalized such that the initial fluorescence intensity = 1, the lowest fluorescence intensity = 0, and rupturing occurred at t = 0. The rupturing curves were fit using Prism5 to a plateau followed by a one-phase decay curve where the plateau value was set to 1. The recovery curves were fit to one-phase associations.

To quantify the ratio of fluorescence intensity between the PN and the MN from images of fixed cells, the plane where the entire PN or MN was in focus was first selected from a 0.5 μm-step z-section. Analysis was based on a previously described method (Hoffman et al., 2001) and began by selecting the chromatin area based on DAPI labeling and measuring the area ($A_I$) and integrated density of fluorescence ($F_I$) of the selection for each PN and MN pair using Photoshop. The area of selection was then expanded by at least 2x and a second group of area and fluorescence measurements taken ($A_O$ and $F_O$). The background subtracted fluorescent intensity values were obtained using the following formula: $F_I - ((F_O-F_I)/(A_I/A_O)) = F\_{N}$. MN fluorescence intensity was normalized to PN intensity and area by using $F_{PN}/(A_{I\text{-}PN}/A_{I\text{-}MN}) = F_{PN\text{-}C}$

and then $F_{MN}/F_{PN-C}$. For analyzing fluorescence at the nuclear rim, the same method was used except that the DAPI selection was converted to a 3-5 px border around the rim.

To determine whether two or more proportions were significantly different between two or more categories of MN, we used Fisher's exact (for a 2x2 table) or $\chi^2$ analysis on the raw data to obtain the p-value with the null hypothesis that all populations had the same proportions. For comparisons with a significant p-value, phi (Cramer's) correlation co-efficient was calculated to determine the degree to which two variables correlated. To account for experimental differences, each experiment was repeated in full at least 3 times with 100 MN analyzed per category each time, except where the N < 300. To determine if there was a significant difference between data obtained in each replicate, p-values were calculated for each replicate. If the p-values were homogenous between replicates, then the raw data was pooled a final p-value calculated. In no case were greater than 4 replicates required to obtain three homogenous populations.

**Supplemental references**


Anderson, D.J., and Hetzer, M.W. (2008). Reshaping of the endoplasmic reticulum limits the rate for nuclear envelope formation. J Cell Biol *182*, 911–924.

Anderson, D.J., Vargas, J.D., Hsiao, J.P., and Hetzer, M.W. (2009). Recruitment of functionally distinct membrane proteins to chromatin mediates nuclear envelope formation in vivo. J Cell Biol *186*, 183–191.

Bodoor, K., Shaikh, S., Salina, D., Raharjo, W.H., Bastos, R., Lohka, M., and Burke, B. (1999). Sequential recruitment of NPC proteins to the nuclear periphery at the end of mitosis. Journal of Cell Science *112 ( Pt 1*, 2253–2264.

Doucet, C.M., Talamas, J.A., and Hetzer, M.W. (2010). Cell cycle-dependent differences in nuclear pore complex assembly in metazoa. Cell *141*, 1030–1041.

Hoffman, D.B., Pearson, C.G., Yen, T.J., Howell, B.J., and Salmon, E.D. (2001). Microtubule-dependent Changes in Assembly of Microtubule Motor Proteins and Mitotic Spindle Checkpoint Proteins at PtK1 Kinetochores. Mol. Biol. Cell *12*, 1995–2009.

Kuga, T., Nozaki, N., Matsushita, K., Nomura, F., and Tomonaga, T. (2010). Phosphorylation statuses at different residues of lamin B2, B1, and A/C dynamically and independently change throughout the cell cycle. Experimental Cell Research *316*, 2301–2312.

Pines, J., and Hunter, T. (1990). Human cyclin A is adenovirus E1A-associated protein p60 and behaves differently from cyclin B. Nature *346*, 760–763.

Schmitz, M.H.A., Held, M., Janssens, V., Hutchins, J.R.A., Hudecz, O., Ivanova, E., Goris, J., Trinkle-Mulcahy, L., Lamond, A.I., Poser, I., et al. (2010). Live-cell imaging RNAi screen identifies PP2A-B55alpha and importin-beta1 as key mitotic exit regulators in human cells. Nature Cell Biology *12*, 886–893.

Schumacher, J., Reichenzeller, M., Kempf, T., Schnolzer, M., and Herrmann, H. (2006). Identification of a novel, highly variable amino-terminal amino acid sequence element in the nuclear intermediate filament protein lamin B(2) from higher vertebrates. FEBS Lett *580*, 6211–6216.

Steigemann, P., Wurzenberger, C., Schmitz, M.H.A., Held, M., Guizetti, J., Maar, S., and Gerlich, D.W. (2009). Aurora B-mediated abscission checkpoint protects against tetraploidization. Cell *136*, 473–484.

Vargas, J.D., Hatch, E.M., Anderson, D.J., and Hetzer, M.W. (2012). Transient nuclear envelope rupturing during interphase in human cancer cells. Nucleus *3*, 88–100.

Supplemental Figure 1

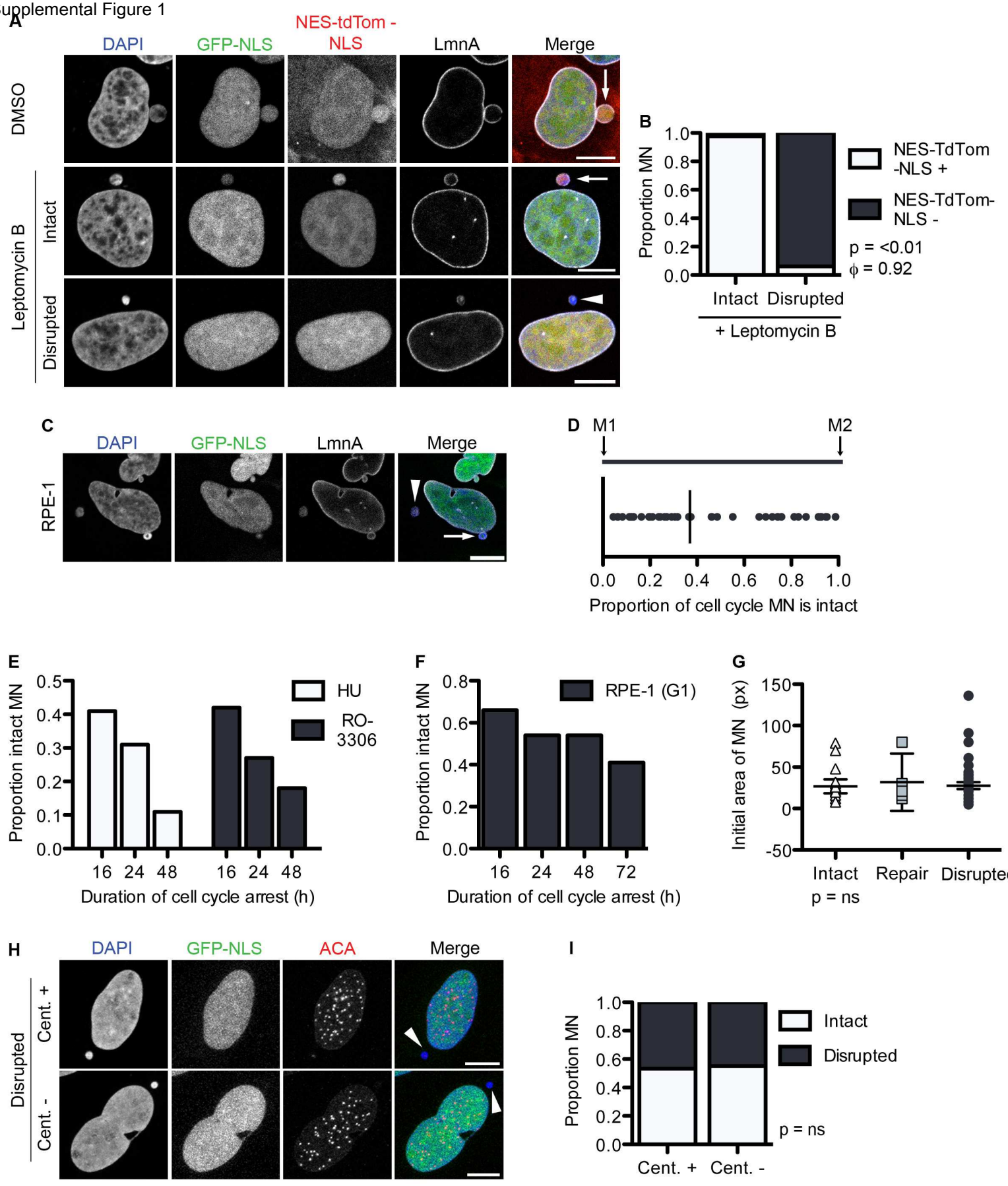


Hatch et al. Supplemental figure 1: Disrupted MN cannot retain nuclear proteins, are present in RPE-1 cells, and occur throughout interphase and independently of MN size or origin, related to figure 1.

Supplemental Figure 2

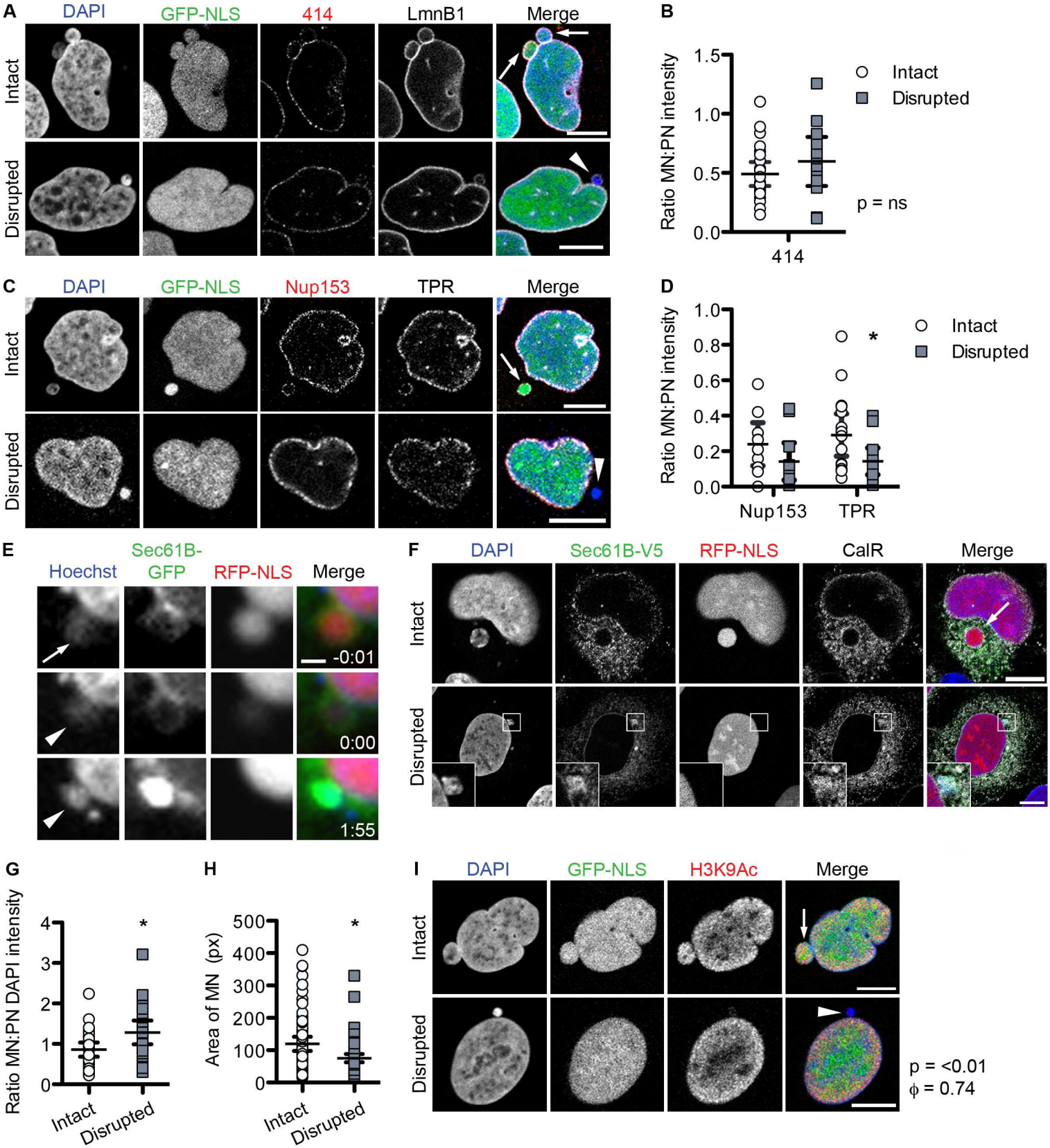


Hatch et al Supplemental figure 2: Disrupted MN retain some nucleoporins, have compacted chromatin, and accumulate a transmembrane ER protein, related to figure 2. .

Supplemental Figure 3

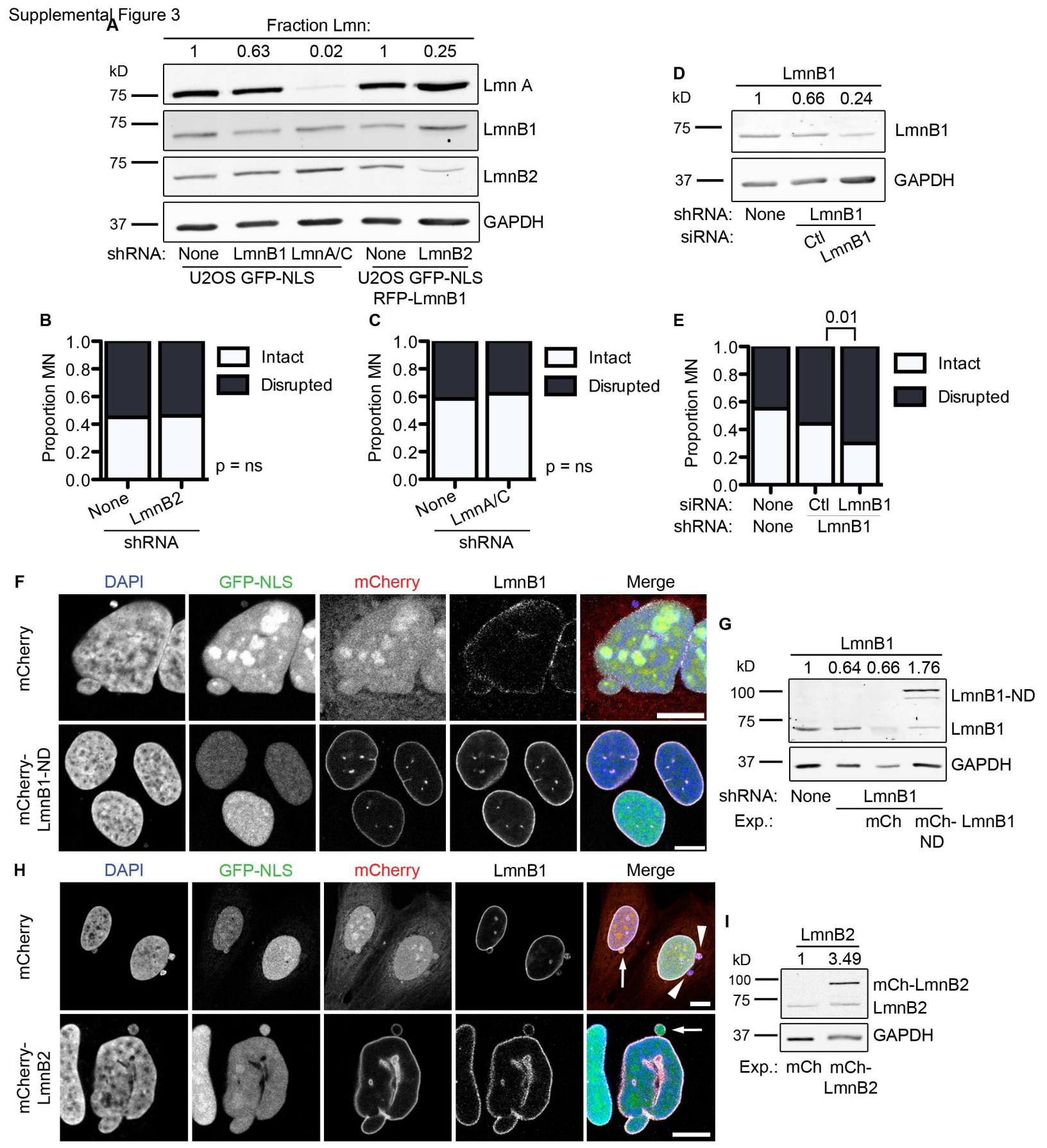


Hatch et al Supplemental figure 3:MN disruption is not affected by loss of lamins A or B2 and controls related to figure 3.

Supplemental Figure 4

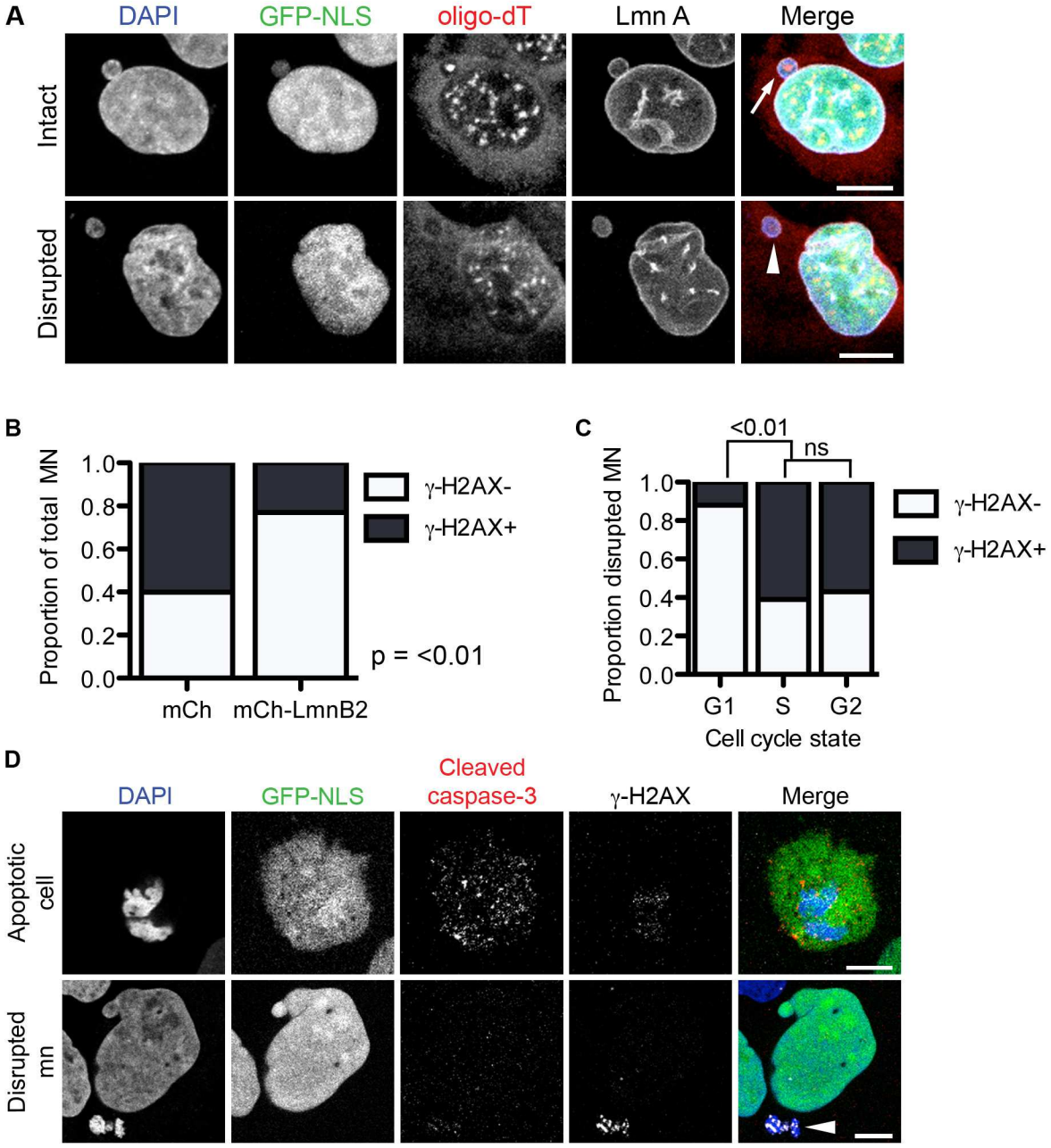


Hatch et al Supplemental figure 4: Disrupted MN fail to transcribe mRNA, are not associated with apoptosis, and show cell-cycle dependent γ-H2AX accumulation, related to figure 4.

Supplemental Figure 5

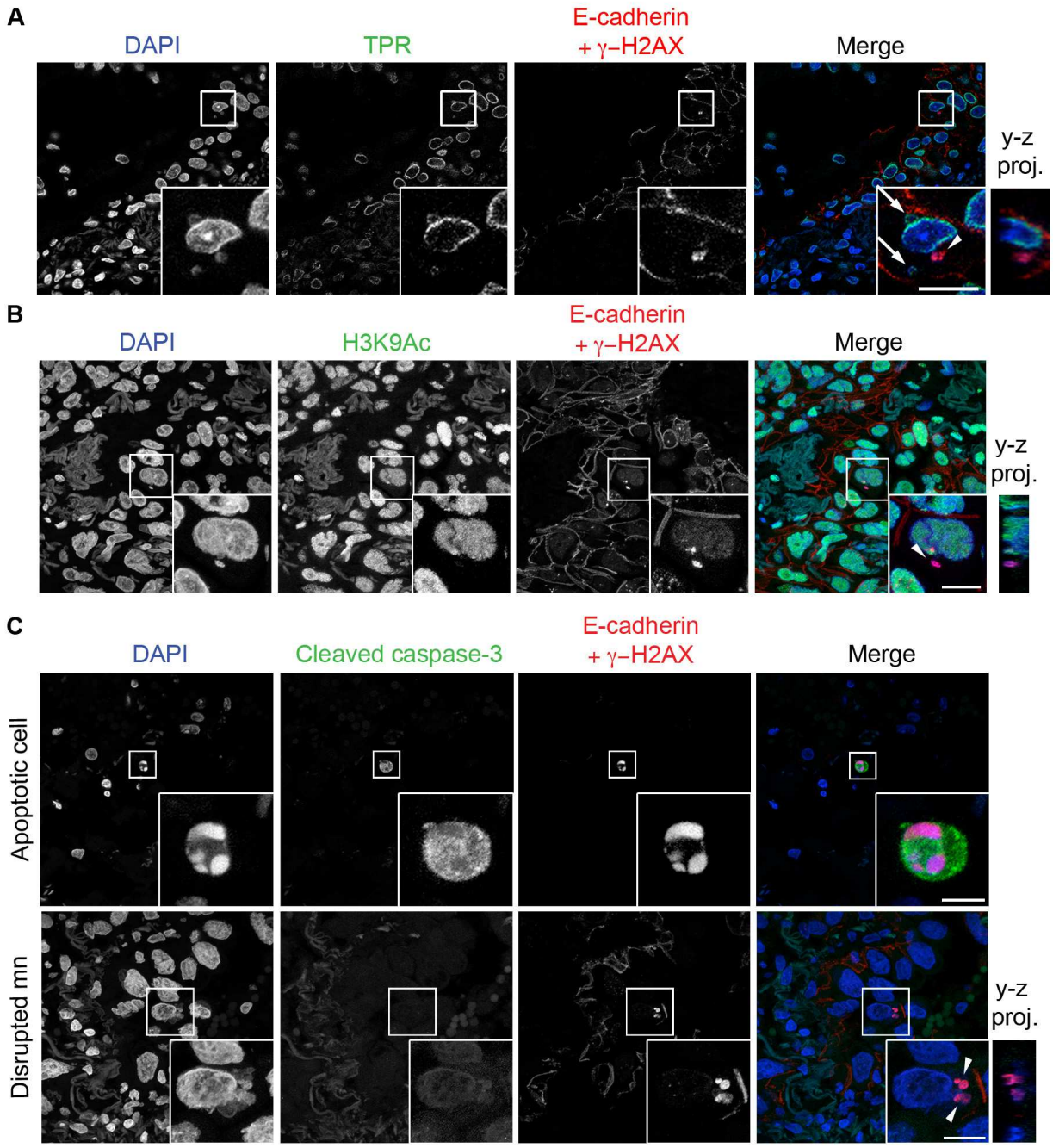


Hatch et al Supplemental figure 5: Disrupted mn in NSCLC lose TPR and acetyl-histone3-K9 and are not associated with apoptotic cells, related to figure 6.